Thermomechanical properties and fatigue of nanocrystalline Ni/Cu electrodeposits

Olivier Arnould, Olivier Hubert, François Hild

▶ **To cite this version:**

Olivier Arnould, Olivier Hubert, François Hild. Thermomechanical properties and fatigue of nanocrystalline Ni/Cu electrodeposits. Material Research Society Spring Meeting, Apr 2004, San Francisco, United States. pp.P7.8.1-6, 10.1557/PROC-821-P7.8 . hal-01961195

HAL Id: hal-01961195
https://hal.science/hal-01961195

Submitted on 21 Jun 2022

HAL is a multi-disciplinary open access archive for the deposit and dissemination of scientific research documents, whether they are published or not. The documents may come from teaching and research institutions in France or abroad, or from public or private research centers.

L'archive ouverte pluridisciplinaire **HAL**, est destinée au dépôt et à la diffusion de documents scientifiques de niveau recherche, publiés ou non, émanant des établissements d'enseignement et de recherche français ou étrangers, des laboratoires publics ou privés.

Thermomechanical properties and fatigue of nanocrystalline Ni/Cu electrodeposits

Olivier Arnould[1], Olivier Hubert and François Hild
LMT-Cachan, ENS Cachan/CNRS UMR 8535/Université Paris VI
61, avenue du Président Wilson
94235 Cachan Cedex, France

ABSTRACT

This study deals with the long-term reliability of a high precision pressure sensor using bellows mainly made of electroplated Ni. Thermomechanical properties of this deposit are obtained by several experiments and compared to theoretical models, computations and other authors' results. Bellows are expected to stay in service for many decades, thus their high cycle fatigue behavior has to be known. Stress-life fatigue curve for crack initiation and fatigue crack growth in the electroplated Ni are measured and identified using numerical computations. Results are compared with other results obtained on similar Ni electrodeposits. Normalized stress-life fatigue curve shows no specific nanosize effects.

INTRODUCTION

This papers deals with the study of aging modes of a high precision pressure sensor. It uses bellows to convert pressure variations into a displacement (figure 1a). The stiffness and airtightness of bellows require to use a Ni/Cu/Ni layered material (overall thickness ~50µm) obtained by electroforming (figure 1b). The main aging mode of this layered material [1] that affects the bellows airtightness is due to high cycle fatigue crack initiation at the surface of the nickel layers and, to a lesser extent, on its propagation through them. The fatigue behavior of the Ni deposits is linked to their microstructure and the associated (thermo)mechanical properties that depend on the electrodeposition process.

NI DEPOSIT CHARACTERIZATIONS

Microstructure analysis

Nickel is electrodeposited in a sulfamate bath ($[Ni(SO_3NH_2)_2 \cdot 4H_20]$ = 600g/l, pH = 4, $\theta = 50°C$) with a low DC-current density ($4 \leq i \leq 10 mA/cm^2$). Deposits are electroplated on a rotating aluminum mandrel first coated with a copper layer. Both are removed at the end of the electrodeposition process to obtain the bellows. Under these conditions, nickel deposits have a fine columnar structure parallel to the electroplating direction (figure 1b) with clusters (figure 2a, [2]) made of micrometer domains of low-misoriented grains (figure 2b). XRD measurements and TEM observations (figure 2c) lead to a mean grain size of about 60nm, small second order residual stresses and a very low dislocation density. Moreover, the plating conditions induce a specific inhibited growth of the nickel layers associated with hydrogen absorption [3]. This yields a (relatively low) $\langle 110 \rangle$ fiber texture along the electroplating direction (figure 1c) and a high (nano)porosity, $f > 5\%$ (density measurements), of the deposits.

[1] now at LMGC, Université de Montpellier II, cc 048, Place Eugène Bataillon, 34095 Montpellier Cedex 05, France
E-mail : arnould@lmgc.univ-montp2.fr

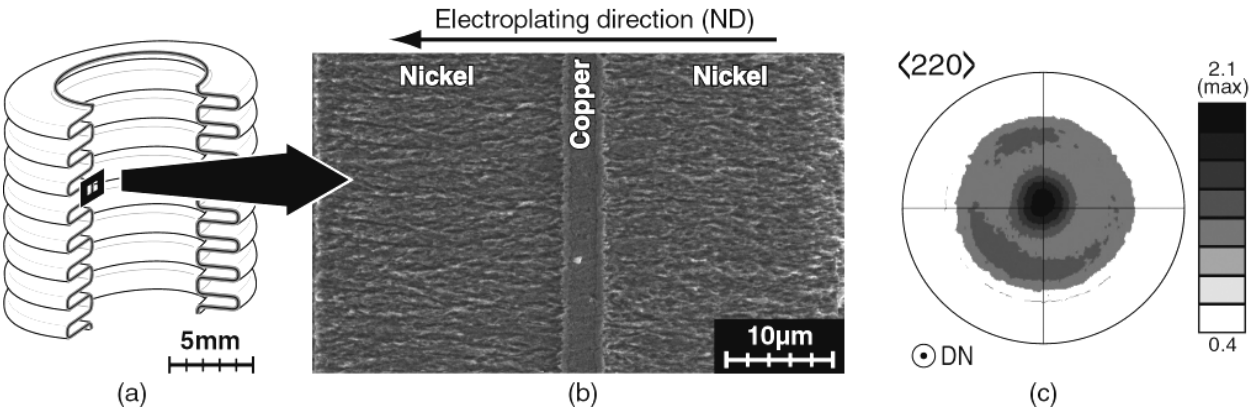

Figure 1. a) General view of electroplated bellows. b) Micrograph of a cross-section obtained in an SEM after chemical etching: fine columnar microstructure of the nickel layers. c) $\langle 220 \rangle$ pole figure obtained by DRX at the surface of the deposit.

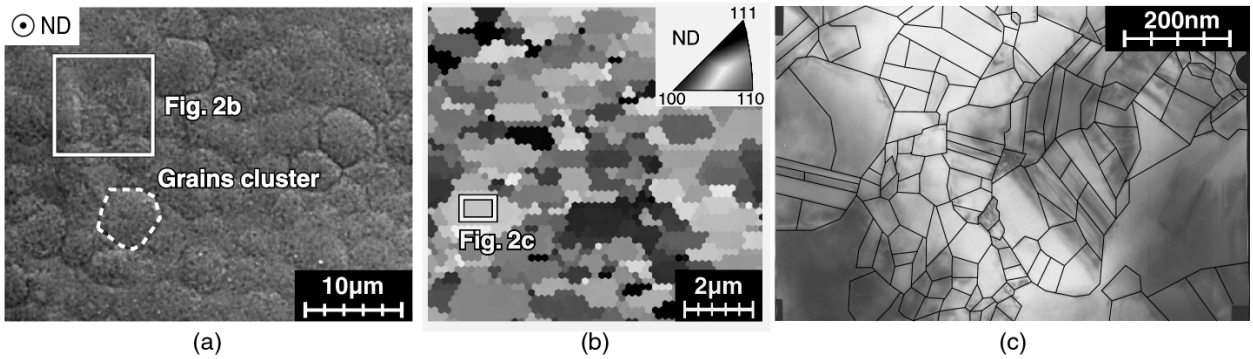

Figure 2. a) SEM micrograph of an electropolished nickel layer surface: detail of a micrometric grains cluster boundary. b) Low angle misorientation domains of (nanometer) grains obtained by EBSD mapping (measurement step: 0.2µm, grey level corresponds to a crystallographic orientation given in the inverse pole figure) at the surface of the Ni deposit. c) Bright field TEM micrograph showing the bimodal nanometer grains. (Sub)Grain boundaries are informatically drawn for a sake of clarity.

The nickel layers give the needed stiffness for the bellows but their porosity is too high to provide the required airtightness. A continuous, *i.e.,* airtight, copper layer (thickness ~3µm) is added between the nickel layers to this aim. This configuration does not modify the effective stiffness of bellows as it allows for the minimization of the *softening* effect of copper since bending is the predominant loading pattern. These microstructural characteristics induce specific thermomechanical properties that have been evaluated and compared to micromechanical models.

Thermomechanical properties

An atypical isotropic thermoelastic behavior, due to the weak fiber texture, has been shown experimentally [1, 4]. The coefficient of thermal expansion (CTE), α, is found to be greater than

its usual value for nickel (*e.g.,* $\alpha(100°C) \approx 17.10^{-6}$ instead of about 14.10^{-6}). The origin of this behavior is still questionable in the present case, *i.e.,* thermoelastic homogenization shows that the porosity does not induce a change in the CTE and the (nano)size effect of the grain is still unclear [5, 6]. The grain size is "too high" to yield a significant change in the elastic properties [7]. The porosity is the main factor that yields a Young's modulus, E = 160GPa, less than the theoretical value of 230GPa (obtained by self-consistent elastic homogenization) for the given fiber texture [8]. Similar Young's moduli have been obtained by Buchheit *et al.* [9] for nickel deposits with a similar $\langle 110 \rangle$ fiber texture obtained with Watt's baths.

Tensile tests (figure 3a), on a specific nickel electrodeposited sheet (figure 3b), with digital image correlation measurements to evaluate the strains, are used to identify a yield strength at 0.02% plastic strain, σ_y, of the order of 600MPa, an ultimate tensile strength, σ_u, of 1.2GPa and a low plastic strain to failure of 1.6%. This is a usual behavior for this kind of material [7, 9]. Figure 3c shows the ductile fracture surface observed on a Ni sample. The measured yield stress is in good agreement with the Hall-Petch relationship [10] when considering the coefficients of the annealed nickel [11] and the mean grain size determined herein. Note that the present mean grain size is too high to lead to a reverse Hall-Petch behavior of the Ni deposits [7].

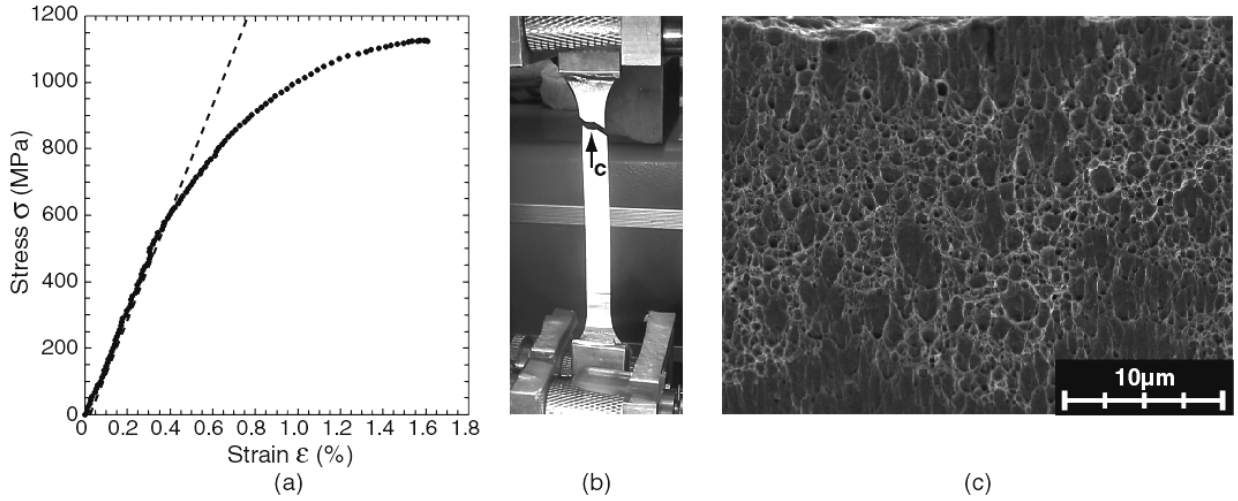

Figure 3. a) Typical stress-strain curve obtained on a Ni deposit sheet. b) View of the *post-mortem* Ni sheet sample in the tensile test device. c) SEM micrograph of the fracture surface.

FATIGUE PROPERTIES

As long-term bellows airtightness is concerned, a specific high cycle fatigue device, put in a resonant testing machine, has been designed [12]. It allows us to carry out high cycle fatigue tests of ten bellows at the same time. Tests are controlled in displacement, u, with a zero mean value, $\overline{u}$, and $\Delta u/2$ its maximum reached during a cycle (*i.e.,* half displacement range). The bellows airtightness is continuously monitored with a pressure sensor. Airtightness loss corresponds to the number of cycles for crack initiation, N_I, as the number of cycle for the crack propagation through the bellows thickness is negligible.

Crack initiation

Stress-life fatigue, *S-N*, curve for crack initiation consists in plotting an equivalent damage stress range $\Delta\sigma^*$ [12] as a function of the number of cycles for the loss in airtightness. $\Delta\sigma^*$ is computed at the most loaded point(s) of bellows by using bi-dimensional (axisymmetric) finite element (FE) analyses for a given cycle. The results are scattered. During a fatigue test, structure and material heterogeneities lead to localized microplasticity and damage phenomena in various sites whereas the whole structure remains elastic. If we assume that these sites are randomly distributed, independent and that crack initiation occurs at the weakest one, the cumulative crack initiation probability, *p*, within bellows Ω, can be described, at endurance, by a two-parameter Weibull model [13, 14]

$$p = 1 - \exp\left[-\frac{V_{eff}}{V_0} \left(\frac{\hat{\sigma}}{\sigma_0} \right)^m \right], \tag{1}$$

where *m* is the Weibull modulus, V_0 a reference volume and σ_0 the scaling stress. $\hat{\sigma}$ is the maximum equivalent stress during a cycle, of period *T*, over the whole structure Ω, *i.e.,* $\hat{\sigma} = \max_{\Omega} (\max_{t\in[0,T]} \sigma^*)$. This model accounts for the stress heterogeneity and volume effects observed during fatigue testing with V_{eff}, the effective volume, defined by

$$V_{eff} = \int_{\Omega} \left(\max_{t\in[0,T]} \sigma^* \Big/ \hat{\sigma} \right)^m \mathrm{d}V \,. \tag{2}$$

This allows us to use other authors' fatigue results obtained with a different sample geometry and scale. Our stress ranges are corrected to have the same effective volume and stress loading ratio, *i.e.,* R_σ = -1 (using the Goodman relationship [15]), as Boyce *et al.* [16]. All stress ranges are furthermore normalized by the yield strength to take the material microstructure into account. The dependence of the number of cycle for crack initiation, N_I, to the stress range, σ_r^*, is modeled with a simple two-parameter, *A* and *n*, Stromeyer law [15]

$$N_I(p) = A \Big/ \left[\Delta\sigma^* - 2\sigma_\infty(p) \right]^n , \tag{3}$$

where $\sigma_\infty(p)$ is the fatigue limit, for a given crack initiation probability, *p*, equal to $\hat{\sigma}$ at endurance. The parameters of the whole modeling are identified on our results and those of Boyce *et al.* [16]. The corresponding curves are reported in figure 4a where an *a priori* estimation of the mean fatigue stress threshold $\bar{\sigma}_\infty$ has been evaluated by using an infrared thermographic technique [17]. A good agreement between the different results and the identified model is shown. The mean fatigue limit, $\bar{\sigma}_\infty$, is such that $\bar{\sigma}_\infty / \sigma_y \approx 2/3$ and $\bar{\sigma}_\infty / \sigma_u \approx 1/3$ that is in agreement with results obtained with usual grain sized nickel [16]. The minimum number of cycles needed to reach the endurance domain is of the order of 10^8-10^9. That means that no specific nanosize effect seems to occur on the fatigue life of the present electroplated nickel.

Crack propagation

Tests have been carried on during some thousands of cycles, N_P, after the airtightness loss to study the crack propagation in electroplated Ni. Results are reported in figure 4b. The fatigue crack growth rate is roughly constant (about 100nm/cycle). Stress intensity factors at the crack tip for different crack lengths have been computed by a three-dimensional FE analysis [12]. A stress intensity factor proportional to the crack length, similar to the case of an orthoradially cracked hollow cylinder [18], is observed. The crack propagation rate is constant while the stress intensity factor increases for values ranging from 5 to 12 MPa.m$^{1/2}$ [12]. This behavior seems to be linked to nickel oxidation, at room temperature, at the crack tip as observed by Boyce *et al.* [16]. Constant crack growth rates for a given stress intensity factor range in the subcritical regime are, for example, observed in glassy materials in corrosive environments [19]. In this case the corrosive species diffusion to the crack tip yields a *constant* crack propagation velocity. SEM observations of the fatigue crack (figures 5a and b) show a transgranular fracture with a two-scale roughness well correlated, for the first one, with the grains cluster size and, for the second one, with the crack growth rate (close to one grain size per cycle).

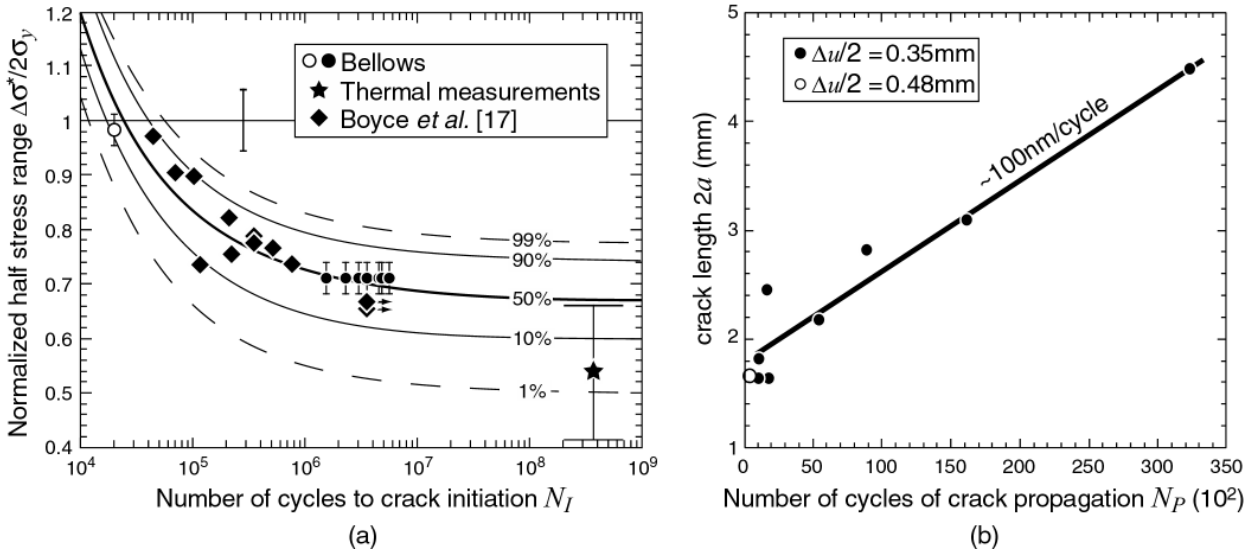

Figure 4. a) Stress-life fatigue curve for crack initiation with R_σ = -1 and $V_{eff} \approx 4.10^{-4}$mm^3. b) Fatigue crack growth for different displacement loading ranges and crack lengths.

CONCLUSIONS

Long-term airtightness of Ni/Cu/Ni electroplated bellows is studied. It is caused by fatigue crack initiation in the nickel layers. Nickel deposits are made of porous micrometer clusters of low-misoriented nanometer grains showing a weak fiber texture along the plating direction. Fatigue crack initiation curves have been measured and modeled using a probabilistic approach. The fatigue behavior of nickel electrodeposits exhibits no specific nanosize effect. Furthermore, constant fatigue crack growths have been measured for different values of the stress intensity factor. This phenomenom seems to be linked to an oxidation mechanism at the crack tip. This assumption must be confirmed by additional investigations.

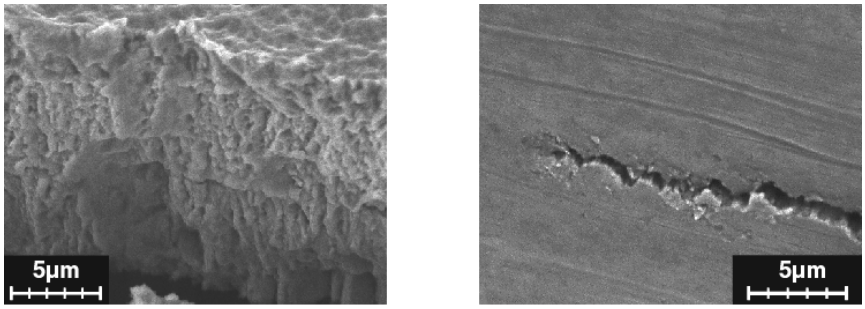

Figure 5. a) SEM micrograph of a fatigue fracture surface showing a roughness length scale close to 100nm. b) SEM micrograph of a fatigue crack tip: highlights of numerous crack deviations with a mean length scale close to the size of the low-misoriented grains domains (figure 2b).

ACKNOWLEDGEMENTS

The authors wish to thank I. Guillot (UTC Compiègne, France) for the TEM observations and V. Ji & W. Seiler (LM3 ENSAM Paris, France) for the XRD characterizations.

REFERENCES

1. O. Arnould and F. Hild, *Defect and Diffusion Forum* **203-205**, 61-80 (2002).
2. S.W. Banovic, K. Barmak and A.R. Marder, *J. Mater. Sci.* **33**, 639-645 (1998).
3. C.S. Lin, P.C. Hsu, L. Chang and C.H. Chen, *J. Appl. Electrochem.* **31**, 925-933 (2001).
4. J. Jumel, F. Taillade and F. Lepoutre, *Eur. Phys. J. – Appl. Phys.* **23**, 217-225 (2003).
5. H. Gleiter, *Prog. Mat. Sci.* **33**, 223-315 (1989).
6. T. Turi and U. Erb, *Mat. Sci. Eng.* **A204**, 34-38 (1995).
7. N. Wang, Z. Wang, K.T. Aust and U. Erb, *Mater. Sci. Eng.* **A237**, 150-158 (1997).
8. G.E. Fougere, L. Riester, M. Ferber, J.R. Weertman and R.W. Siegel, *Mater. Sci. Eng.* **A204**, 1-6 (1995).
9. T.E. Buchheit, D.A. La Van, J.R. Michael, T.R. Christenson and S.D. Leith, *Metall. Mater. Trans.* **33A**, 539-554 (2002).
10. Hall, E.O., *Proc. Phys. Soc.* **B64**, 747-753, (1951) and Petch, N.J., *J. Iron Steel Inst.* **174**, 25-28 (1953).
11. Website: neons.mems.cmu.edu/rollett/rollett.html
12. O. Arnould, PhD thesis, University of Paris VI (2003). Website: tel.ccsd.cnrs.fr
13. W. Weibull, *Roy. Swed. Inst. Eng. Res.* **151** (1939).
14. F. Hild, R. Billardon and A.S. Béranger, *Mech. Mat.* **22**, 11-21 (1996).
15. S. Suresh, *Fatigue of Materials*, Cambridge University Press (1991).
16. B.L. Boyce, J.R. Michael and P.G. Kotula, *Acta Mater.* **52(6)**, 1609-1619 (2004).
17. M.P. Luong, *Mech. Mat.* **28**, 155-163 (1998).
18. Murakami, Y., *Stress intensity factors handbook*, vol. 2, Pergamon Press, Oxford (1981).
19. A.K. Varshneya, *Fundamental of inorganic glasses*, Academic Press, Boston (1994).